Computational Mechanics 33 (2004) 154–163 © Springer-Verlag 2003
DOI 10.1007/s00466-003-0514-4

Identification of cracks and cavities using the topological sensitivity boundary integral equation

R. Gallego, G. Rus

Abstract The purpose of this communication is to present a novel approach to compute the so called *Topological Sensitivity* (TS) of any variable or functional in elasticity using Boundary Integral Equations (BIE's), and its use as a tool for identification of defects, by itself or in conjunction with zero-order methods, like Genetic Algorithms. The TS of a cost functional provides a measure of the susceptibility of a defect being at a given location. The main contributions are summarized in the following points:

- Computation of the TS based on a linearized topological expansion, using Boundary Integral Equations. The TS is computed using only information of the non-damaged domain. The calculation is carried out for circular cavities or straight cracks, but the procedure is extensible to other kinds of defects.
- It is shown that the topological expansion provides a very accurate tool for estimating the defect sizes, even for very large flaws, relative to the domain size.
- Applicability of the TS for identification of defects, by itself or associated with Genetic Algorithm. This association is very advantageous since the computational time is dramatically reduced.

Keywords Topological derivative, Two-dimensional elastostatics, Boundary integral equations, Boundary element method, Defect identification, Genetic algorithms

1 Introduction

A direct problem can be stated as the calculation of the response (certain displacements u and stress vectors q) in a specific body defined by its geometry (domain Ω and boundary Γ), mechanical properties (k), behavior model (operator L) and boundary conditions (some known values of u and q). As a counterpart of this, an inverse problem (IP) is one in which part of the information above is unknown, for instance part of the geometry, its mechanical properties, etc, which has to be computed with the aid of extra information about the response of the body to a set of known excitations. In this paper the so called identification inverse problem is dealt with, where the unknown variable is part of the geometry, actually, the location and size of internal flaw(s).

When seeking defects or flaws inside a body, any physical magnitude that propagates within and that manifests on an accessible part of it might be considered in order to obtain information about what is happening inside. In this paper the elastostatic response of a two-dimensional body is considered, although the ideas presented here are readily extended to elastodynamics.

In general, an IP is cast as an appropriate optimization problem for a residual functional which depends on the difference between the measured data and the computed ones. The computation of the functional gradient with respect to the shape parameters has been extensively studied, to be used in conjunction to standard minimization procedures. However in this paper a different approach is presented which consists in devising a domain function, the so called *Topological Sensitivity* (TS), whose minimum pinpoints the location and size of the sought flaw. The location of the TS minimum is performed using a Genetic Algorithm (GA).

The use of GA or Evolutionary Algorithms (EA) in general, for identification of flaws, within the framework of Boundary Integral Equation procedures, have been explored by different authors in the past decade, (Koguchi and Watabe, 1997; Kowalckzyk et al., 1998; Tanaka and Nakamura, 1994; Stavroulakis and Antes, 1998b; Stavroulakis and Antes, 1998a; Stavroulakis, 2001). In all these papers the functional to be optimized is the full residual, instead of its TS, and therefore the computation is very costly.

The idea of *Topological Sensitivity* was first introduced by Eschenauer et al. (1994) (they called "bubble method"), for compliance minimization in twodimensional elastostatic problems, and was latter generalized and exploited for shape inverse problem by Sokolowski and coworkers (Sokołowski and żochowski, 1998; Jackowska-Strumiło et al., 1999; Lewiński and Sokołowski, 1997) for circular and non-circular flaws. Garreau et al. (2001) developed the idea for a general arbitrary-shaped flaw in the context of elastostatics, as well. In those papers an adjoint state method is employed to obtain the topological derivative whereas a direct approach fully based in Boundary Integral Equations (BIE) is presented in this paper. The procedure can be easily extended to flaws of any shape as is demonstrated extending the idea for crack-like flaws. Furthermore, other than Neumann boundary conditions can be considered within the flaw or even the creation of *inclusions* instead of voids.

Received: 20 December 2002 / Accepted: 26 September 2003
Published online: 15 December 2003

R. Gallego (✉), G. Rus
Department of Structural Mechanics,
University of Granada, E-18071, Spain
e-mail: gallego@ugr.es

The computation of the TS for an arbitrary functional using a BIE is presented is this paper for the first time, and a procedure is devised to greatly enhance the applicability of zero-order methods, as Genetic Algorithms, since the use of the TS as an internal steps on one hand reduce the number of design parameters, and on the other, eliminate the need of computing a distinct direct problem for each individual (design parameter values) during the search.

2
Topological sensitivity

The topological derivative of a shape functional provides information about the variation of the functional due to creation of a small hole centered at a given location x_0. Formally, given a shape functional,

$$\mathscr{J} : \Omega \to \mathscr{R} \tag{1}$$

for a given domain Ω, and denoting by $B_r(x_0)$ a closed ball of radius $r > 0$ centered at x_0, the topological derivative is defined as,

$$\mathscr{J}^*(x_0) = \lim_{r \to 0^+} \frac{\mathscr{J}(\Omega \backslash B_r(x_0)) - \mathscr{J}(\Omega)}{\|B_r(x_0)\|} \tag{2}$$

or alternatively,

$$\bar{\mathscr{J}}^*(x_0) = \lim_{r \to 0^+} \frac{\mathscr{J}(\Omega \backslash B_r(x_0)) - \mathscr{J}(\Omega)}{r^\alpha} \tag{3}$$

provided that such limits exist; α is the dimension of the space, 2 or 3.

For plane problems ($\alpha = 2$), an equivalent definition can be obtained introducing the function of the small parameter $r \geq 0$, $J(r) = \mathscr{J}(\Omega \backslash B_r(x_0))$, and compute its expansion around $r = 0^+$,

$$J(r) = J(0^+) + \frac{r^2}{2} J''(0^+) + o(r^2) \tag{4}$$

Then, $J''(0^+)$, is equivalent to $\mathcal{J}^*(x_0)$, save for a multiplicative constant.

It is important to stress that the topological derivative is not the *shape* derivative of a functional with respect to the size of a void, since the expansion is performed from a flawless domain.

From this, the *Topological Sensitivity* of the functional J is defined as the differential,

$$\delta \mathscr{J}(x_0) = \bar{\mathscr{J}}^*(x_0) \delta A \tag{5}$$

where δA is the size of a small flaw centered at x_0.

In this paper, a BIE is developed for the computation of the TS of tractions and displacements on the boundary Γ of an arbitrary domain Ω subject to whatever boundary conditions, using only information from the Non-damaged State (NS). The NS is defined over the same domain, without flaws, and with the same boundary conditions. From the TS of the boundary variables is straightforward to compute the sensitivity of any boundary or domain variable (stresses, strains, etc) and then of any boundary or domain functional.

Furthermore, the definition of the Topological Sensitivity can be extended to vanishing flaws of any shape. In this paper, circular and straight crack-like flaws are considered.

3
Basic boundary integral equations

In a domain Ω bounded by Γ, the displacement integral equation can be written as (Brebbia and Domínguez, 1992):

$$c_k^i(\mathbf{y}) u_k(\mathbf{y}) + \int_\Gamma \left[q_k^i(\mathbf{x};\mathbf{y}) u_k(\mathbf{x}) - u_k^i(\mathbf{x};\mathbf{y}) q_k(\mathbf{x}) \right] \mathrm{d}\Gamma(\mathbf{x}) = 0 \tag{6}$$

where $u_k(\mathbf{x})$ is the kth component of the displacement vector in the actual state at the *observation point* $\mathbf{x}$. $q_k(\mathbf{x}) = \sigma_{jk}(\mathbf{x}) n_j(\mathbf{x})$ is the stress vector in the actual state at point $\mathbf{x}$. $\sigma_{jk}(\mathbf{x})$ is the stress tensor and n_j the outward normal. $u_k^i(\mathbf{x};\mathbf{y})$ is the kth component of the displacement vector at the observation point $\mathbf{x}$ due to a point load applied in direction i at the *collocation point* $\mathbf{y}$ (fundamental solution). $q_k^i(\mathbf{x};\mathbf{y}) = \sigma_{lk}^i(\mathbf{x};\mathbf{y}) n_l(\mathbf{x})$ is the stress vector of the fundamental solution. c_k^i is the free term whose value depends on the position of the collocation point. Thus, $c_k^i(\mathbf{y}) = \delta_k^i$ (Kronecker delta) if $\mathbf{y} \in \Omega \backslash \Gamma$; if $\mathbf{y} \in \Gamma$, $c_k^i(\mathbf{y})$ depends on the angle θ subtended by the left and right tangents at $\mathbf{y}$, and is such that $c_k^i(\mathbf{y}) = 1/2 \delta_k^i$ when $\theta = 180^\circ$ (smooth boundary); $c_k^i(\mathbf{y}) = 0$ otherwise.

Using boundary collocation and proper discretization of the ensuing BIE, the former equation can be solved, providing the unknown displacements and tractions along the boundary. The displacements at any location within the domain can be computed using the same equation, as a post-processing step. Likewise, the stress tensor at any point $\mathbf{y} \in \Omega \backslash \Gamma$ can be evaluated using the corresponding integral equation, which is obtained from Eq. (6) by application of the Hooke's law $\sigma_{ij}(\mathbf{y}) = \lambda \delta_{ij} u_{m,m}(\mathbf{y}) + \mu(u_{i,j}(\mathbf{y}) + u_{j,i}(\mathbf{y}))$, leading to,

$$\sigma_{ij}(\mathbf{y}) + \int_\Gamma \left[d_{jk}^i(\mathbf{x};\mathbf{y}) q_k(\mathbf{x}) - s_{jkl}^i(\mathbf{x};\mathbf{y}) n_l(\mathbf{x}) u_k(\mathbf{x}) \right] \times \mathrm{d}\Gamma(\mathbf{x}) = 0 \quad \mathbf{y} \in \Omega \backslash \Gamma \tag{7}$$

where the new kernels are given by,

$$d_{jk}^i(\mathbf{x};\mathbf{y}) = \lambda \delta_{ij} u_{k,m}^m(\mathbf{x};\mathbf{y}) + \mu(u_{k,j}^i(\mathbf{x};\mathbf{y}) + u_{k,i}^j(\mathbf{x};\mathbf{y}))$$

$$s_{jkl}^i(\mathbf{x};\mathbf{y}) = \lambda \delta_{ij} \sigma_{kl,m}^m(\mathbf{x};\mathbf{y}) + \mu(\sigma_{kl,j}^i(\mathbf{x};\mathbf{y}) + \sigma_{kl,i}^j(\mathbf{x};\mathbf{y}))$$

Note that the comma in the above kernel definitions stands for the derivative with respect to the observation point coordinates.

It is worth recalling that the computation of stresses by Eq. (7) does not entail the solution of a new system of equations, nor the integration of singular or hypersingular kernels, and is therefore computationally inexpensive.

3.1
Topological sensitivity boundary integral equation

The Topological Sensitivity Boundary Integral Equation is computed considering a modified state that contains an infinitesimal flaw (Damaged State or DS). In an

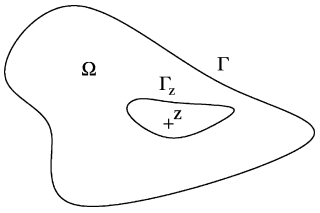

Fig. 1. Perturbed domain due to the appearance of a infinitesimal cavity

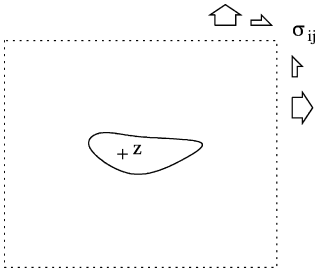

Fig. 2. An infinitesimal flaw in an infinite domain subject to a uniform remote stress field

homogeneous domain Ω whose exterior boundary is Γ, and subject to arbitrary boundary conditions, consider the appearance of a stress free cavity centered at point $\mathbf{z}$ whose boundary is Γ_z, which surrounds the domain Ω_z, as shown in Fig. 1.

The standard boundary integral equation given in Eq. (6) can be applied to this problem, splitting the boundary integration in two parts, Γ and Γ_z:

$$c_k^i(\mathbf{y})\tilde{u}_k(\mathbf{y}) + \int_\Gamma \left[q_k^i(\mathbf{x};\mathbf{y})\tilde{u}_k(\mathbf{x}) - u_k^i(\mathbf{x};\mathbf{y})\tilde{q}_k(\mathbf{x})\right]\mathrm{d}\Gamma(\mathbf{x}) + \int_{\Gamma_z} \left[q_k^i(\mathbf{x};\mathbf{y})\tilde{u}_k(\mathbf{x}) - u_k^i(\mathbf{x};\mathbf{y})\tilde{q}_k(\mathbf{x})\right]\mathrm{d}\Gamma(\mathbf{x}) = 0 \tag{8}$$

The tilde over the variables denotes that their values are modified due to the appearance of the infinitesimal flaw.

Considering the condition $\tilde{q}_k = 0$ along Γ_z, the equation simplifies into,

$$c_k^i(\mathbf{y})\tilde{u}_k(\mathbf{y}) + \int_\Gamma \left[q_k^i(\mathbf{x};\mathbf{y})\tilde{u}_k(\mathbf{x}) - u_k^i(\mathbf{x};\mathbf{y})\tilde{q}_k(\mathbf{x})\right]\mathrm{d}\Gamma(\mathbf{x}) + \int_{\Gamma_z} q_k^i(\mathbf{x};\mathbf{y})\tilde{u}_k(\mathbf{x})\mathrm{d}\Gamma(\mathbf{x}) = 0 \tag{9}$$

Now, the displacements on the flaw's boundary can be split as,

$$\tilde{u}_k(\mathbf{x}) = u_k^0 + \delta\bar{u}_k(\mathbf{x})$$

where u_k^0 is a rigid-solid displacement and $\delta\bar{u}_k(\mathbf{x})$ a movement relative to the center, due to the local state of stresses. Then, the integral along Γ_z transforms into,

$$\begin{aligned}\int_{\Gamma_z} q_k^i(\mathbf{x};\mathbf{y})u_k(\mathbf{x})\mathrm{d}\Gamma(\mathbf{x}) &= u_k^0 \int_{\Gamma_z} q_k^i(\mathbf{x};\mathbf{y})\mathrm{d}\Gamma(\mathbf{x}) \\ &\quad + \int_{\Gamma_z} q_k^i(\mathbf{x};\mathbf{y})\delta\bar{u}_k(\mathbf{x})\mathrm{d}\Gamma(\mathbf{x}) \\ &= \int_{\Gamma_z} q_k^i(\mathbf{x};\mathbf{y})\delta\bar{u}_k(\mathbf{x})\mathrm{d}\Gamma(\mathbf{x})\end{aligned} \tag{10}$$

since the fundamental solution stresses along a close path are self-equilibrated.

To first order the stresses at any point inside $\Omega\backslash\Omega_z$, far from the flaw location, are equal to those of the Primary State, $\sigma_{ij}(\mathbf{x})$, and therefore, the displacements $\delta\bar{u}_k(\mathbf{x})$ along the vanishing flaw are equal to those due to a uniform remote stress field in an infinite plate, as shown in Fig. 2.

More formally,

$$\tilde{\sigma}_{ij}(\mathbf{x}) = \sigma_{ij}(\mathbf{z}) + \text{h.o.t.} \tag{11}$$

for $\mathbf{x}$ far from $\mathbf{z}$, where h.o.t stands for *higher order terms*, and,

$$\delta\bar{u}_k(\mathbf{x}) = \delta u_k^\infty(\mathbf{x}) + \text{h.o.t.} \tag{12}$$

where $\delta u_k^\infty(\mathbf{x})$ represents the solution of the problem given in Fig. 2, due to the stresses $\sigma_{ij}(\mathbf{z})$. Note that expansion in Eq. (11) holds only in order to compute $\delta u_k^\infty(\mathbf{x})$.

On the other hand, on Γ_z,

$$q_k^i(\mathbf{x};\mathbf{y}) = \sigma_{jk}^i(\mathbf{x};\mathbf{y})n_j(\mathbf{x}) = \sigma_{jk}^i(\mathbf{z};\mathbf{y})n_j(\mathbf{x}) + \text{h.o.t.} \tag{13}$$

The integral along the flaw boundary turns therefore into,

$$\int_{\Gamma_z} q_k^i(\mathbf{x};\mathbf{y})\tilde{u}_k(\mathbf{x})\mathrm{d}\Gamma(\mathbf{x}) = \sigma_{jk}^i(\mathbf{z};\mathbf{y}) \int_{\Gamma_z} n_j(\mathbf{x})\delta u_k^\infty(\mathbf{x})\mathrm{d}\Gamma(\mathbf{x}) + \text{h.o.t.} \tag{14}$$

The ensuing integral implies the solution of a simple auxiliary problem over an infinite domain.

Subtracting the resulting BIE for the DS to Eq. (9), the BIE for the NS, the following equation is obtained,

$$c_k^i(\mathbf{y})\delta u_k(\mathbf{y}) + \int_\Gamma \left[q_k^i(\mathbf{x};\mathbf{y})\delta u_k(\mathbf{x}) - u_k^i(\mathbf{x};\mathbf{y})\delta q_k(\mathbf{x})\right]\mathrm{d}\Gamma(\mathbf{x}) = -\sigma_{jk}^i(\mathbf{z};\mathbf{y}) \int_{\Gamma_z} n_j(\mathbf{x})\delta u_k^\infty(\mathbf{x})\mathrm{d}\Gamma(\mathbf{x}) \tag{15}$$

where $\delta u_k(\mathbf{y})$ and $\delta q_k(\mathbf{y})$ are the topological sensitivities of displacements and tractions on the boundary, due to the appearance of an infinitesimal arbitrarily shaped flaw at $\mathbf{z}$.

Equation 15 is termed *Topological Sensitivity Boundary Integral Equation* (TSBIE).

Note that the auxiliary problem can be solved using non-dimensional variables, $x^* = x/\delta L$, $y^* = y/\delta L$, $u_k^{*\infty} = \delta u_k^\infty/\delta L$, where δL is a characteristic length of the flaw. Doing that the equation turns into,

$$c_k^i(\mathbf{y})\delta u_k(\mathbf{y}) + \int_\Gamma \left[q_k^i(\mathbf{x};\mathbf{y})\delta u_k(\mathbf{x}) - u_k^i(\mathbf{x};\mathbf{y})\delta q_k(\mathbf{x})\right] \mathrm{d}\Gamma(\mathbf{x}) = -\delta L^2 \sigma_{jk}^i(\mathbf{z};\mathbf{y}) \int_{\Gamma_z^*} n_j(\mathbf{x}^*) u_k^{*\infty}(\mathbf{x}^*) \mathrm{d}\Gamma^*(\mathbf{x}^*) \tag{16}$$

The right hand side integral in Eq. (15) can be performed analytically in the case of simple flaw shapes as is shown in the next sections.

3.2
Topological sensitivity BIE for circular flaws

In case the flaw is circular the auxiliary problem has analytical solution. The displacements along the circular boundary are,

$$\delta u_1^\infty = \frac{\delta R}{E}\left[(3\sigma_{11} - \sigma_{22})\cos\theta + 4\sigma_{12}\sin\theta\right]$$
$$\delta u_2^\infty = \frac{\delta R}{E}\left[(-\sigma_{11} + 3\sigma_{22})\sin\theta + 4\sigma_{12}\cos\theta\right]$$

or,

$$\begin{pmatrix}\delta u_1^\infty \\ \delta u_2^\infty\end{pmatrix} = \frac{\delta R}{E}\begin{pmatrix}3\sigma_{11} - \sigma_{22} & 4\sigma_{12} \\ 4\sigma_{12} & 3\sigma_{22} - \sigma_{11}\end{pmatrix}\begin{pmatrix}\cos\theta \\ \sin\theta\end{pmatrix} \tag{17}$$

where δR is the radius of the cavity, E the elastic modulus, and θ is the usual polar coordinate.

Since the outward normal on Γ_z is $\mathbf{n} = -(\cos\theta, \sin\theta)^{\mathrm{T}}$, the displacement can be finally written as,

$$\delta u_k^\infty = -\delta R \Sigma_{kl} n_l \tag{18}$$

where Σ_{kl} is a constant matrix which depends on the value of $\sigma_{ij}(\mathbf{z})$ and the elastic modulus.

Then the integral along the flaw boundary can be performed:

$$\begin{aligned}\int_{\Gamma_z} q_k^i(\mathbf{x};\mathbf{y})\tilde{u}_k(\mathbf{x})\mathrm{d}\Gamma(\mathbf{x}) &= -\delta R \sigma_{jk}^i(\mathbf{z};\mathbf{y})\Sigma_{kl}(\mathbf{z}) \int_{\Gamma_z} n_j(\mathbf{x}) n_l(\mathbf{x}) \mathrm{d}\Gamma(\mathbf{x}) \\ &= -\pi\delta R^2 \sigma_{jk}^i(\mathbf{z};\mathbf{y})\Sigma_{kl}(\mathbf{z})\delta_{jl} \\ &= -\delta A\ \sigma_{jk}^i(\mathbf{z};\mathbf{y})\Sigma_{kj}(\mathbf{z})\end{aligned} \tag{19}$$

where $\delta A = \pi\delta R^2$ is the area of the flaw.

In conclusion, generalizing to M circular cavities centered at a set of points $\mathbf{z}^j$ the TSBIE can be written as,

$$c_k^i(\mathbf{y})\delta u_k(\mathbf{y}) + \int_\Gamma \left[q_k^i(\mathbf{x};\mathbf{y})\delta u_k(\mathbf{x}) - u_k^i(\mathbf{x};\mathbf{y})\delta q_k(\mathbf{x})\right] \times \mathrm{d}\Gamma(\mathbf{x}) = \sum_{j=1}^{M} {}^t U^i(\mathbf{z}^j;\mathbf{y})\delta A_j \tag{20}$$

where,

$${}^t U^i(\mathbf{z}^j;\mathbf{y}) = \sigma_{jk}^i(\mathbf{z}^j;\mathbf{y})\Sigma_{kj}(\mathbf{z}^j) \tag{21}$$

and,

$$(\Sigma_{kj}) = \frac{1}{E}\begin{pmatrix}3\sigma_{11} - \sigma_{22} & 4\sigma_{12} \\ 4\sigma_{12} & 3\sigma_{22} - \sigma_{11}\end{pmatrix} \tag{22}$$

3.3
Topological sensitivity BIE for straight cracks

A similar expression is obtained when the vanishing flaw is a crack-like defect. Using a local coordinate system, centered at the crack, such that the y' axis is perpendicular to the crack faces, the solution of the auxiliary problem is,

$$\delta u_1'^\infty = \frac{2\sigma_{12}'(1-\nu^2)}{E}\sqrt{\delta a^2 - x'^2}$$
$$\delta u_2'^\infty = \frac{2\sigma_{22}'(1-\nu^2)}{E}\sqrt{\delta a^2 - x'^2} \tag{23}$$

where δa is the half-length of the crack.

Performing the integral along the crack boundary,

$$\int_{\Gamma_z}\left(n_j'\delta u_k'^\infty\right)\mathrm{d}\Gamma(\mathbf{x}) = \frac{2\pi\delta a^2(1-\nu^2)}{E}\begin{pmatrix}0 & 0 \\ \sigma_{12}' & \sigma_{22}'\end{pmatrix} \tag{24}$$

is obtained, and transforming this expression to global coordinates the integral on the flaw leads to,

$$\int_{\Gamma_z} q_k^i(\mathbf{x};\mathbf{y})\tilde{u}_k(\mathbf{x})\mathrm{d}\Gamma(\mathbf{x}) = -{}^t U^i(\mathbf{z};\mathbf{y})\delta A \tag{25}$$

where,

$${}^t U^i(\mathbf{z}^j;\mathbf{y}) = \sigma_{jk}^i(\mathbf{z};\mathbf{y})\Sigma_{kl}(\mathbf{z}) \tag{26}$$

and Σ_{kl} is given now by the expression,

$$(\Sigma_{kl}) = \frac{2\pi(1-\nu^2)}{E} \times \begin{pmatrix}-\sigma_{12}'\sin\theta\cos\theta + \sigma_{22}'\sin\theta^2 & -\sigma_{22}'\sin\theta\cos\theta - \sigma_{12}'\sin\theta^2 \\ -\sigma_{22}'\sin\theta\cos\theta + \sigma_{12}'\cos\theta^2 & +\sigma_{12}'\sin\theta\cos\theta - \sigma_{22}'\cos\theta^2\end{pmatrix} \tag{27}$$

where, in turn, σ_{ij}' is the local stress tensor on the crack reference system:

$$\sigma_{22}' = \frac{\sigma_{11} + \sigma_{22}}{2} + \frac{\sigma_{22} - \sigma_{11}}{2}\cos 2\theta - \sigma_{12}\sin 2\theta \tag{28}$$

$$\sigma_{12}' = \frac{\sigma_{22} - \sigma_{11}}{2}\sin 2\theta + \sigma_{21}\sin 2\theta \tag{29}$$

and, in this case $\delta A = \delta a^2$.

It is worth stressing that the equations Eq. (20) and Eq. (21) are therefore valid both for circular flaws and

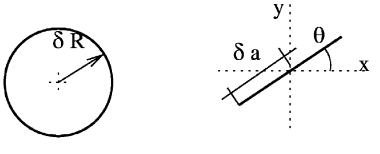

Fig. 3. Description of the circular cavity and crack

cracks, or actually for an arbitrary shaped flaw, using for each case the corresponding value of δA and Σ_{kl}.

4 Numerical solution of the topological de-rivative boundary integral equation

Using standard discretization techniques the TSBIE is transformed into an algebraic system of equations,

$$\mathbf{M}\delta\mathbf{v} = {}^{t}\Delta\delta\mathbf{A} \tag{30}$$

Note that the integral operator for δu_k and δq_k in Eq. (15) is the same that the operator for the NS in Eq. (6), and therefore, the system matrix $\mathbf{M}$ is the same than for the computation of boundary displacements and tractions of the Non-damaged State; $\delta\mathbf{v}$ collects the variation values corresponding to the non prescribed displacements and stresses on the boundary. ${}^{t}\Delta$ is a $n \times m$ matrix, where n is the number of collocation points and m is the number of flaws. To compute this matrix just the values of the Non-damaged State stress tensor at the location of the flaws are needed. Therefore, to set the system of equations Eq. (30) there is no need to discretize any flaw boundary, i.e., only the solution of the Non-damaged State is necessary; $\delta\mathbf{A}$ is a vector with the 'areas' of the flaws.

Solving $\mathbf{M}$ for each column of ${}^{t}\Delta$ the *Topological Jacobian*, ${}^{t}\mathbf{J}$, is defined by the equation

$$\mathbf{M}{}^{t}\mathbf{J} = {}^{t}\Delta \tag{31}$$

and therefore, the TS's of the boundary variables are computed by,

$$\delta\mathbf{v} = {}^{t}\mathbf{J}\delta\mathbf{A} \tag{32}$$

In this paper, isoparametric quadratic elements have been employed, both for the solution of the Non-damaged State and the discretization of the Topological Sensitivity BIEs.

5 Identification of flaws using the topological sensitivity

In order to search for unknown flaws inside a domain using experimental information of the behavior of the medium, a standard procedure consists in setting a number of tentative flaws inside the body and compute the variables (displacement, traction, strain, ...) at the same locations where the experimental values are retrieved. The difference, residual, between the computed values $\mathbf{v}$ and the experimentally measured ones $\mathbf{v}^{\exp}$ is then minimized with respect to some geometrical variables, design variables, which define the location and size of the flaws. Note that to apply this procedure it is necessary to solve and discretize the problem *with the assumed cavities* in each iteration of the minimization process. The topological sensitivity provides a mean to *dramatically reduce the computational effort* since, for a given location of the flaws, the problem with flaws can be solved *using only the solution of the Non-damaged State*, as shown in the next subsection.

5.1 Optimum flaw size estimation

Given the position of a number of flaws, a cost functional can be defined from the residual $\mathbf{R} = \mathbf{v}^{\exp} - \mathbf{v}(\mathbf{A}(\mathbf{z}_j))$ as $f = \frac{1}{2}\mathbf{R}^{\mathrm{T}}\mathbf{R}$. The following reasoning, however, can be applied whatever be the cost functional. The topological expansion for the residual is,

$$\begin{aligned}\mathbf{R}(\mathbf{A}(\mathbf{z}_j)) &= \mathbf{v}^{\exp} - \mathbf{v}(\mathbf{A}(\mathbf{z}_j)) \approx \mathbf{v}^{\exp} - \mathbf{v}(0) - \delta\mathbf{v} \\ &= \Delta\mathbf{v} - {}^{t}\mathbf{J}(\mathbf{z}_j)\delta\mathbf{A}\end{aligned} \tag{33}$$

where $\Delta\mathbf{v} = \mathbf{v}^{\exp} - \mathbf{v}(0)$ is readily computed once the Non-damaged State is solved. Using this expansion, the functional f can be approximated by,

$$\begin{aligned}f &= \frac{1}{2}\mathbf{R}^{\mathrm{T}}\mathbf{R} \approx \frac{1}{2}(\Delta\mathbf{v} - {}^{t}\mathbf{J}(\mathbf{z}_j)\delta\mathbf{A})^{\mathrm{T}}(\Delta\mathbf{v} - {}^{t}\mathbf{J}(\mathbf{z}_j)\delta\mathbf{A}) \\ &= f(0) + \delta f\end{aligned} \tag{34}$$

where, $f(0) = \frac{1}{2}\Delta\mathbf{v}^{\mathrm{T}}\Delta\mathbf{v}$, and,

$$\delta f = \frac{1}{2}\delta\mathbf{A}^{\mathrm{T}}{}^{t}\mathbf{J}^{\mathrm{T}}{}^{t}\mathbf{J}\delta\mathbf{A} - \delta\mathbf{A}^{\mathrm{T}}{}^{t}\mathbf{J}^{\mathrm{T}}\Delta\mathbf{v} \tag{35}$$

is the Topological Sensitivity of the cost functional.

The minimum of the approximate functional is attained for the following flaw sizes,

$$\delta\mathbf{A} = ({}^{t}\mathbf{J}^{\mathrm{T}}{}^{t}\mathbf{J})^{-1}{}^{t}\mathbf{J}^{\mathrm{T}}\Delta\mathbf{v} \tag{36}$$

Note that the matrix to be inverted is small, only $m \times m$, where m is the number of flaws, just a scalar in case only one flaw is sought after.

If accurate, these size estimates can be used in conjunction of any minimization algorithm, providing several advantages:

- The solution of a direct problem *is carried out once for the whole search, regardless of the number and location of the flaws*. Only the Non-damaged Problem has to be discretized, and therefore only one system matrix, $\mathbf{M}$, has to be computed and factored.
- The computational time of each iteration is *dramatically reduced* in comparison with the solution of multiple direct problem, since:
  - To obtain the topological Jacobian ${}^{t}\mathbf{J}$ the right hand side matrix ${}^{t}\Delta$ in equation Eq. (30) has to be computed, but this implies just the calculation of the tensors $\Sigma_{jk}(\mathbf{z}_j)$ which basically involves the computation of the stresses of the NS at points $\mathbf{z}_j$. Actually, the whole stress field could be computed at the start of the algorithm in a fine enough mesh of points, and afterwards compute the stresses at any location by interpolation.
  - Next, the system in Eq. (31) is to be solved, but $\mathbf{M}$ is already factorized and ready for forward and back substitution, once for each flaw.
- The number of design parameters is reduced since the optimum $\delta\mathbf{A}$ is computed in an inner step, and only the center (and angle in the case of cracks) of each flaw are included within the design variable vector.

The ability to easily include several simultaneous flaws gives the possibility of searching an undefined number of defects by allowing for a number of flaws in excess, and letting the non existing flaws vanish by themselves.

5.2 Verification of optimum flaw size estimation

To verify the validity of the first order topological approximation of the residual for optimum flaw size

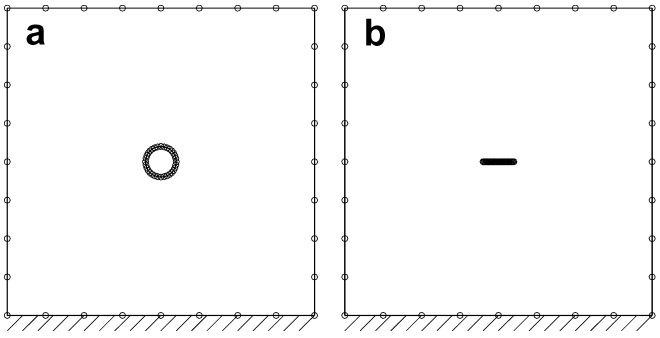

Fig. 4. Geometry of benchmark problems for a circular cavity (a) and a crack (b)

estimation, two simple benchmark problems are presented. In both cases a 2×2 square domain under non-symmetric boundary conditions is considered. The flaw is a centered circular cavity with radius R in the first case, and a centered crack with half-length a in the second, as shown in Fig. 4.

The bottom edge is fixed, and a parabolic load is applied along the right side of magnitude $(t_x, t_y) = (1, 1)$ on its center and (0,0) on the corners. The "experimental" measurements are the displacements along the same right vertical edge.

The boundary is discretized by four quadratic elements per edge. The experimental values are simulated, and are actually computed solving the problem with the real flaw, although this step is obviously unnecessary in case real experimental measures are available.

The problems have been solved for different sizes of the flaw, from a very small one, R or $a \approx 10^{-8}$ to a very large one R or $a \approx 0.8$. Note that in this last case the cavity occupies almost the whole domain, or in the case of the crack, it almost divides the domain in two parts.

In Fig. 5 the estimated size of the flaw (δR for the cavity to the left, and δa for the crack to the right) is represented versus the real one (R or a). There is a perfect one to one correlation. The differences appear only for very small sizes, due to numerical errors, and very large ones, due to the importance of higher order terms in the topological expansion.

It is shown then, that the topological expansion provides a extremely good estimation of the flaw size for a very large range of sizes. This fact points to the possibility of using this tool for a wider class of problems in the mechanics of solids with defects, since it can reduce the computational time for solving problems with a large number of flaws.

5.3
Verification of the topological sensitivity accuracy

In this paragraph, the full cost functional is compared to its topological sensitivity in order to assess the validity of the proposed approximation. To do so, both the functional and its sensitivity are computed for different positions of a cavity in the benchmark problem shown in Fig. 4. For the computation of the cost functional the simulated experiment has a centered cavity of radius ($R = 0,1$). The cavity is located at points along a centered horizontal line ($y = 0.0$). For the radius, two alternatives are considered: for the first one the radius is fixed at 0.15 for all positions of the cavity, while for the second one the radius at each position is the optimum predicted by the approach proposed in the preceding subsection.

In Fig. 6 the cost functional and its topological sensitivity are shown vs. the x position of the center of the cavity, for the first case. The figure shows that the topological sensitivity is a very good approximation of the full cost functional. The disagreement is larger the closer is the cavity to the right hand side of the plate. This is due to the fact that the closer is the cavity to the edge, the less accuarate is the hypothesis about the stress field of a cavity in an infinite domain. Nevertheless, note that both curves are very similar and that their minima coincide.

In Fig. 7 both the cost functional and its sensitivity are shown for the second case, where the radius of the cavity at each position is computed optimizing the topological sensitivity. The predicted radius is represented as well. In this case the curves are practically indistinguishable for most of the range. The discrepancy for positions close to the left edge are again due to the loss of accuracy of the infinite domain stress field hypothesis.

Note however that close to the right edge the error is now very small, since in this case the radius of the cavity is smaller than in the first case and therefore the errors due to the linear topological approximation are negligible.

The inlet in the figure shows a zoom of the curves close to the center ($x = 0.0$) to provide a better appreciation of the agreement between the cost functional and its sensitivity.

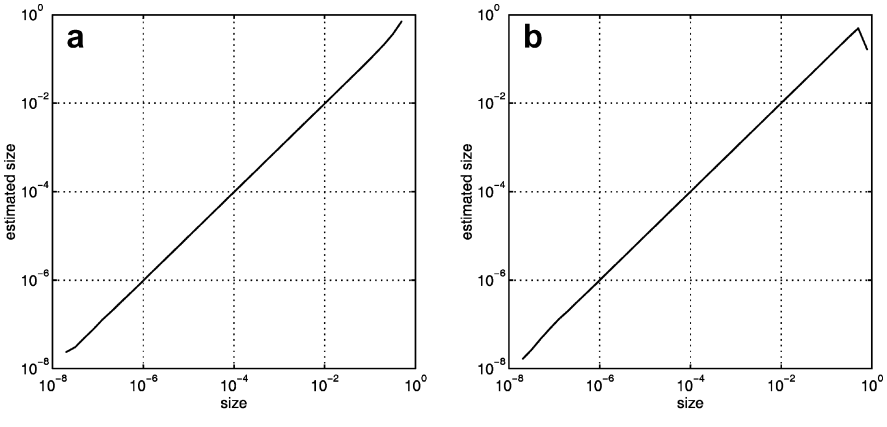

Fig. 5. Correlation of estimated and real flaw size: (a) circular cavity, (b) crack

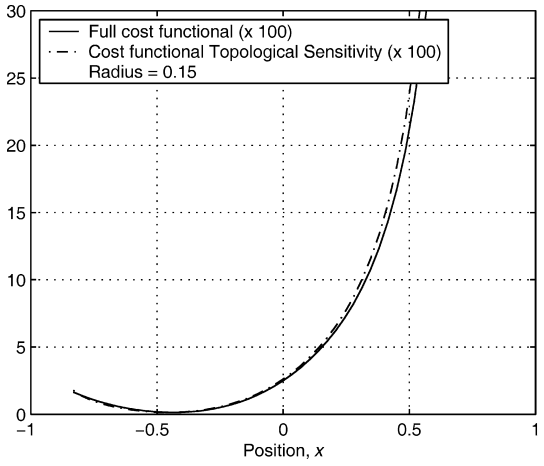

Fig. 6. Comparison of full cost functional vs. topological sensitivity: constant radius $R = 0.15$

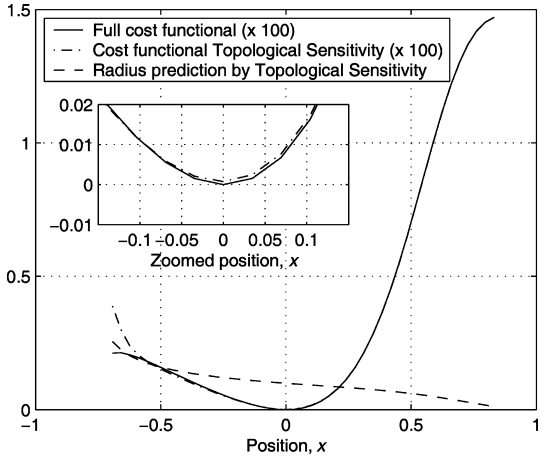

Fig. 7. Comparison of full cost functional vs. topological sensitivity: optimum radius

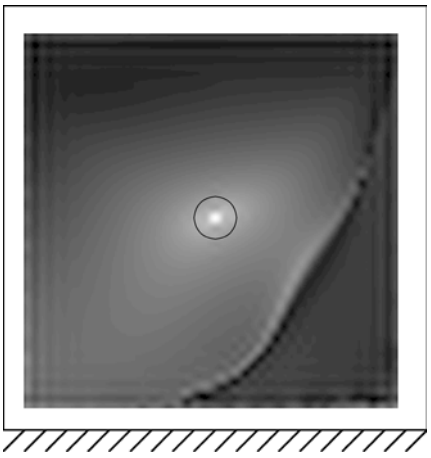

Fig. 8. Cost functional topological sensitivity in the domain for a centered circular cavity

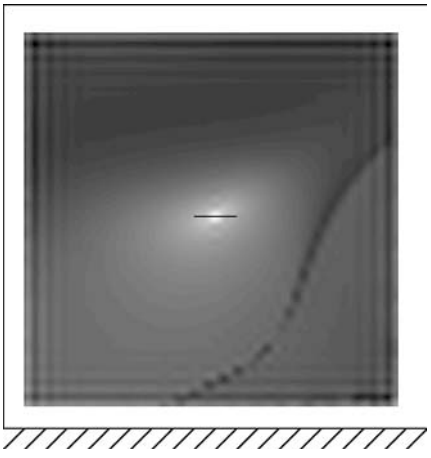

Fig. 9. Cost functional topological sensitivity in the domain for a centered crack

5.4
Location of flaws by minimization of the linearized cost functional

At any locations $\mathbf{z}_j$ within the domain the optimum size of the flaws can be estimated to first topological order as shown in the preceding Sect. 5.2. If the actual linearized cost functional is then computed by,

$$f(0) + \delta f(\mathbf{z}_j) = (\Delta \mathbf{v} - {}^t\mathbf{J}(\mathbf{z}_j)\delta\mathbf{A})^{\mathrm{T}}(\Delta \mathbf{v} - {}^t\mathbf{J}(\mathbf{z}_j)\delta\mathbf{A}) \tag{37}$$

the most probable location of the flaw(s) would be the value(s) of $\mathbf{z}_j$ such that δf attains its minimum value.

Four applications are run to test the validity of this idea. The exterior domain and boundary conditions are those shown in Fig. 4.

In the first two tests there is no modeling nor experimental error. The first one corresponds to a centered circular flaw with radius $R = 0.1$, and the second to a centered crack with half-length $a = 0.1$.

In Fig. 8 the topological sensitivity of the cost functional is shown, superimposed to the geometry of the domain and location of the flaws. The minimum of the Topological Sensitivity exactly pinpoints the presence, location and size of the cavity. It has to be mentioned that the minimum value, attained at the center, is three orders of magnitude larger than its value elsewhere, in absolute value, clearly discriminating the location of the flaw.

Likewise, in Fig. 9, the value of the topological sensitivity of the cost functional is shown, for the case of a centered crack. The result is extremely good, since the value of the linear cost functional detects and localizes the defect unequivocally. The minimum value, at the center, is now even greater than in the previous case.

In the third application, the problem is again the square with a centered circular cavity, but now the simulated experimental values are altered with a 10% error. These experimental errors affect the computation of the estimated size of the flaw through Eq. (36), and then to the topological sensitivity of the cost functional.

The value of the topological sensitivity of the cost functional is shown in Fig. 10. Even with a large error as the one considered, the value of the TS again pinpoints clearly the presence and position of the flaw. The

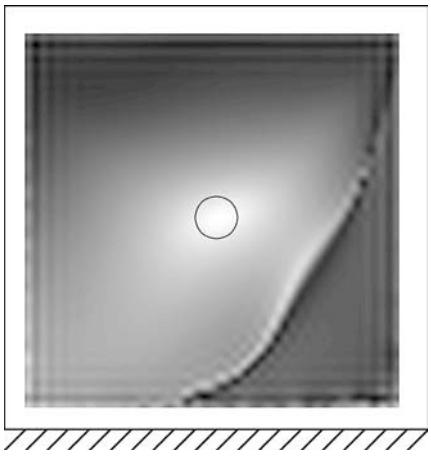

Fig. 10. Cost functional topological sensitivity in the domain for a centered circular cavity, considering a 10% error in the simulated error

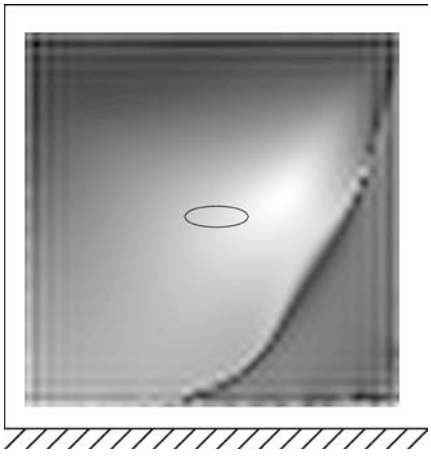

Fig. 11. Cost functional topological sensitivity in the domain for a centered elliptical cavity. The sensitivity is computed assuming a circular flaw

minimum is not as sharp as in the no-error case, and it is not exactly at the center, but nevertheless its value is two order of magnitude larger that elsewhere, and its location is very close to the center. Note that besides this extreme value close to the center, there is a crest-like local extreme, but whose value is 1.5 times lower than the global one, in absolute value.

Finally, a problem with a modeling error is presented. In this case the real flaw is a centered ellipse whose semi-axis are $a = 0.15$ and $b = 0.1$. The boundary conditions are like in previous applications, fixed at the bottom edge, and parabolic load at the right one. The topological sensitivity is computed considering that the sought flaw is a circular cavity. It can be expected, therefore, that the predictions will not be as good as in previous cases.

In Fig. 11 the value of the topological sensitivity is shown. Again, this value detect unequivocally the presence of a flaw. Its location is not pinpointed as precisely as in the other cases, but nevertheless, the extreme of the linearized cost functional is very close to the center.

It has to be born in mind that the expression of the topological sensitivity for elliptical shape flaws can be readily computed. Using such expression it is expected that the location of the flaw would be exactly found, as in the case of circular flaws and cracks.

6
Search of defects by an evolutionary algorithm-topological sensitivity approach

The identification of flaws by Evolutionary Algorithm using BIE have been proposed by a number of authors, as mentioned in the Introduction.

The Evolutionary Algorithms are zero-order methods, i.e. do not use information about the sensitivity or gradient of the functional with respect to the design parameters, and are therefore well suited for problems where this gradient is unavailable, or it is very expensive to compute. The main advantage of these methods is that are global, i.e. explore the whole range of variation of the design variables, but the disadvantage is the large computing time required, since the cost functional has to be evaluated a very large number of times, in comparison with first or higher order minimization approaches.

The use of the topological sensitivity, however, can cut this computational time to a fraction, since the solution of the problems with flaws is found using the optimum size estimate, as shown in the preceding sections.

Within the framework of genetic optimization, the set of design parameters or "phenotype", is encoded as a chain of variables, "chromosomes". A population of test flaws, "individuals", is assumed. For each individual, a fitness function has to be computed. In this case the fitness is defined as $e(x) = -\log f$, so the bigger the error the lower the fitness.

Several steps are implemented for the simulation: first there is a "selection" step where individuals with better fitness are given a higher probability to reproduce. Second a "crossover" operator permits parts of the encoding string of the individual parents to be exchanged within the reproduction step. Finally, in the "mutation" step, arbitrary parts of the information are changed at random during the creation of the new generation. There is a large number of variations and additions to these basic evolutionary steps, but the simplest version is used in this paper, since the objective is not to test the Evolutionary Algorithms for flaw detection, but the improvement raised by their combination with the topological expansion flaw size estimation.

Each individual consists in $2 \times m$ design parameters, the coordinates of the center of the m flaws. Note that the size of the flaw is computed by the topological expansion, and it is therefore removed from the design variable set, reducing the number of unknowns. In the case of cracks, the angle with respect to the x-axis is included as a design parameter.

6.1
Numerical applications for flaw identification by genetic algorithm-topological sensitivity

A simple genetic algorithm has been coded and plugged into the topological sensitivity. The code has been adapted from the one developed by Haataja (2000). The parameters used for all the genetic algorithm runs are,

Number of individuals in population	30
Number of generations	100
Probability of mutation	0.02
Probability of crossover	0.8
Tournament probability	0.7
Scale for mutations	0.1
Gens	Real-coded

In the first two problem, an unique flaw is sought after, a centered circular cavity or a crack. In both cases the algorithm finds exactly the location and size of the flaw. The best individual, superimposed to the real flaw, and evolution of the process is shown in figures Fig. 12 and 13, for the cavity and crack, respectively. To attain convergence about 30 iterations are needed, in the case of the circular cavity, and 100 in the case of the crack. This is due to the fact that there is an extra design parameter, crack angle, in this last case.

Using standard Genetic Algorithm, 100 iterations with 30 individuals per generation entails the solution of $100 \times 30 = 30.000$ distinct direct problems. On the contrary, using the Topological Sensitivity only the Non-damaged State, i.e. the domain with no flaw has to be solved, and each of this 30.000 analysis involves just a forward and back substitution with the factorized system matrix.

The results for a problem with two equal circular cavities are shown in Fig. 14. The best individual is represented to the left, superimposed to the real flaws, and the evolution of the process to the right. To obtain these results, extra simulated experimental measures have been provided: besides the displacements along the right edge, the displacements at the top edge have been included.

In the final application, a centered circular cavity is to be found. However two cavities are considered in the search. In Fig. 15 the best individual and the evolution of the process are shown, to the right and to the left, respectively.

Note that one of the flaws coincides with the actual flaw, while the other one has almost collapsed. Actually, different individuals with similar high fitness consists in a correct centered cavity and a very small flaw randomly located.

7 Conclusions

The Topological Sensitivity (TS) gives the first order variation in the response due to the presence of an infinitesimal flaw. In this paper a Boundary Integral Equation for the computation of the TS has been developed, and fully completed for the cases of circular cavities or crack-like defects.

The TS is a very promising tool for identification of defects since it has been shown that provides a very accurate estimate of the flaw size, using only information of the flawless problem, or Non-damaged State (NS). Actually, the computation of the TS at a given location, just requires the computation of the stresses of the NS, at this point, plus a forward-backward substitution in the NS system of equations.

Furthermore, the TS of the cost functional directly pinpoints the presence, location and size of the defects, and it can be used directly as an identification tool. The

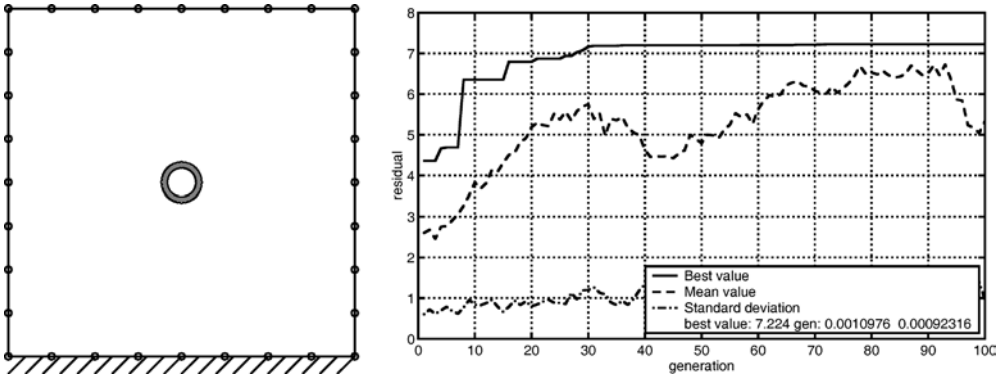

Fig. 12. GA-TS identification of a centered cavity

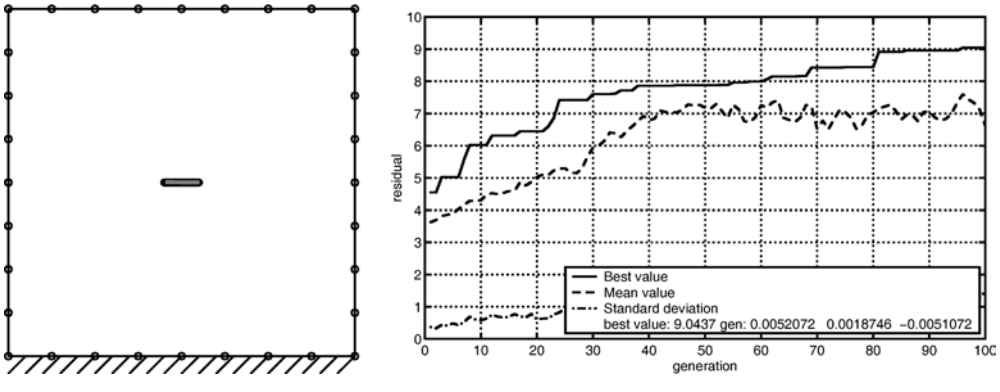

Fig. 13. GA-TS identification of a centered crack

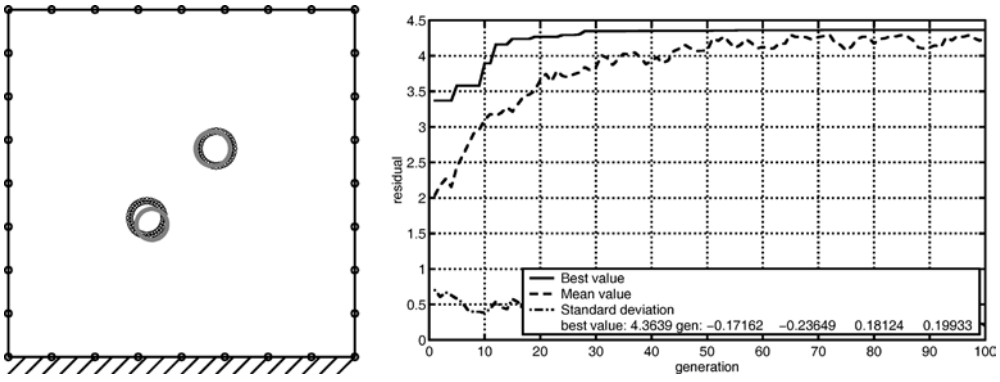

Fig. 14. GA-TS identification of two circular cavities

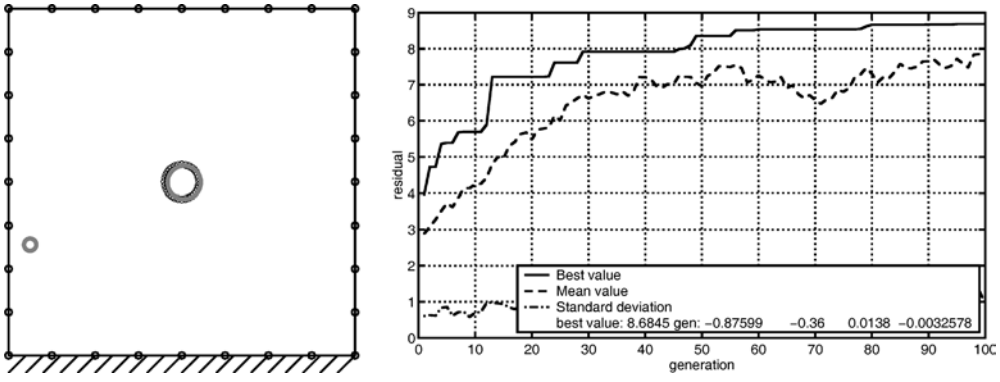

Fig. 15. GA-TS identification of a centered circular cavities. The individuals consist in two cavities

value of the TS is very stable as has been proved in cases with experimental or modeling errors.

In conjunction to zero-order methods as Genetic Algorithm, the use of the TS can greatly enhanced their range of applicability, since the GA-TS approach cuts to a fraction the computational time required. The combined GA-TS method has the following characteristics:

- A unique direct problem computation is needed for the whole search since no discretization or direct solution is needed for the flaws. The direct problem has moreover no flaw.
- The computation of the Topological Sensitivity is based on the already factorized system matrix of the direct problem and on a cheap computation of stresses at the location of the sought defect.
- The size of the flaws is computed by a very accurate linear estimate within the iteration step, reducing significantly the number of parameters. This stabilizes and accelerates the search further.

The ability to obtain the TS for several simultaneous flaws opens large possibilities for the use of this tool for other problems within the mechanics of solids with defects.

References

1. **Brebbia CA, Domínguez J** (1992) Boundary Elements, An Introductory Course. CMP, McGraw Hill
2. **Eschenauer HA, Kobelev VV, Schumacher A** (1994) Bubble method for topology and shape optimization of structures. Struct. Optim. 8: 42–51
3. **Garreau S, Duillaume P, Massmoudi M** (2001) The topological asymptotic for the PDE systems: the elasticity case. SIAM J. Control Optim. 39(6): 1756–1778
4. **Haataja J** (2000) Matlab function for simulating a simple real-coded genetic algorithm. Center for Scientific Computing, Box 405, FIN-02101 Espoo. Internet: Juha.Haataja@csc.fi
5. **Jackowska-Strumiło L, Sokołowski J, Żochowski A** (1999) The topological derivative method and artificial neural networks for numerical solution of shape inverse problems. Rapport de Recherche 3739, Institute National de Recherche en Informatique et en Automatique
6. **Koguchi H, Watabe H** (1997) Improving defects search in structure by boundary element and genetic algorithm scan method. Eng. Anal. Bound. Ele. 19: 105–116
7. **Kowalckzyk T, Fukukawa T, Yoshimura S, Yagawa G** (1998) An extensible evolutionary algorithm approach for inverse problems. In: Tanaka M, Dulikravich GS (eds) Inverse Problems in Engineering Mechanics, p. 541–550
8. **Lewiński T, Sokołowski J** (1997) Topological derivative for nucleation of non-circular voids. Rapport de Recherche 3798, Institute National de Recherche en Informatique et en Automatique
9. **Sokołowski J, Żochowski A** (1998) Topological derivatives for elliptic equations. In: Proc. Inverse Problems, Control and Shape Optimization, p. 129–136
10. **Stavroulakis GE** (2001) Inverse and Crack Identification Problems in Engineering. Kluwer Academic Publishers
11. **Stavroulakis GE, Antes H** (1998a) Crack detection in elastostatics and elastodynamics. a BEM modelling – neural network approach. In: Tanaka M, Dulikravich G (eds) Inverse Problems in Engineering Mechanics
12. **Stavroulakis GE, Antes H** (1998b) Flaw identification in elastomechanics: BEM simulation with local and genetic optimization. Struct. Optim. 16: 162–175
13. **Tanaka M, Nakamura M** (1994) Application of genetic algorithm to plural defects identification. In: Bui H, Tanaka M et al. (eds) Inverse Problems in Engineering Mechanics